PHYSICS AND CHEMISTRY OF SOLID STATE
V. 26, No. 3 (2025) pp. 613-621
Section: Technology

DOI: 10.15330/pcss.26.3.613-621

Vasyl Stefanyk Carpathian National University

ФІЗИКА І ХІМІЯ ТВЕРДОГО ТІЛА
Т. 26, № 3 (2025) С. 613-621
Технічні науки

PACS:47.60.-i

ISSN 1729-4428 (Print)
ISSN 2309-8589 (Online)

I.R. Vashchyshak[1], S.P. Vashchyshak[2], T.M. Mazur[1], M.P. Mazur[1]

Study of the heat transfer efficiency of a wick heat pipe with induction heating of the core made of magnetic stainless steel

[1]*Ivano-Frankivsk National Technical University of Oil and Gas, Ivano-Frankivsk, Ukraine, tetiana.mazur@nung.edu.ua*
[2]*King Danylo University, Ivano-Frankivsk, Ukraine*

The results of mathematical modelling of a heat pipe with induction heating of the core, designed for efficient transfer of low-temperature heat flow to the working fluid in conditions of limited dimensions, are presented. The design includes a thin-walled copper casing, a porous wick structure made of non-magnetic stainless steel mesh, and a magnetic stainless steel core heated by a cylindrical induction coil placed on the casing above the core. Based on physical models of heat transfer, a mathematical description of the processes has been developed that takes into account induction heat generation, the heat capacity of the tube components, and heat losses due to free convection. The dependence of the heating dynamics and thermal efficiency on the angle of inclination of the heat pipe relative to the vertical has been established. The results of the calculations showed that maximum efficiency is achieved in a vertical position, and with an increase in the angle of inclination above 60°, there is an increase in gravitational resistance to fluid motion, which leads to a gradual decrease in heat transfer. It has been shown that at inclinations up to 80°, the performance of the structure is maintained, but to ensure stable operation at even greater angles, additional measures are necessary: reducing the radius of the pores of the wick structure to increase capillary pressure, increasing the thickness or number of mesh layers, and selecting working fluids with more favourable wetting properties. Further work is aimed at experimental verification of the obtained models and optimisation.

Keywords: heat pipe, core, thermal resistance, heat flux, thermal conductivity, resonant circuit, frequency.

Received 10 January 2025; Accepted 15 September 2025.

Introduction

Due to their high thermal conductivity, heat pipes are widely used in various devices for heat transfer, heating, temperature equalisation, etc. [1-4]. Due to the insignificant temperature difference along the length of the body, wick heat pipes can be used as low-temperature heat sources for warming the human body. In [1], the influence of various types of cores on the efficiency of heating the tube body in a vertical orientation was investigated. This allows the optimal material and size of the core to be selected but does not allow us to understand how the temperature of the tube will change when its angle of inclination changes. In addition, the design of the tube and the induction system for heating the coolant were not described theoretically, which does not allow for an accurate assessment of the thermal and energy characteristics of the tube and prediction of their changes.

I. Problem statement

In order to evaluate the influence of various elements of the tube design on its overall thermal resistance, determine the temperature difference along the length of the body, understand the behaviour of the wick heat pipe at different angles of orientation in space, and find the limiting angles of inclination, it is necessary to create a mathematical model of a heat pipe with a porous wick. For fast and efficient heating of the heat pipe, it is necessary to calculate the parameters of the main elements of its induction heating system and simulate the operation of this system in a specialised software environment.

II. Presentation of the main material

The design of a heat pipe with a porous wick and induction heating of the coolant is shown in Fig. 1. It is based on a thin-walled copper tube 1, 0.5 m long, with a diameter of 0.018 m, a wall thickness of $t_{wall} = 1 \cdot 10^{-3}$ m, an inner radius of $r_{in} = 8 \cdot 10^{-3}$ m, sealed at the bottom with a P-shaped copper cover 2. The P-shaped design of the cap allows additional heat to be supplied to the heat pipe from below using a heater 3, the contact area of which with the pipe is covered with thermal paste 4 to improve heat transfer. A frame 5 made of S-Glass aluminosilicate glass with high thermal conductivity and low gas emission for operation in a vacuum is installed inside the lower part of the tube [5]. The frame is $l_{evap} = 3 \cdot 10^{-2}$ m long and $t_{frame} = 3 \cdot 10^{-4}$ m thick. A core 6 made of strips of thin magnetic stainless steel AISI 430 is wound onto it in multiple layers. The core is evenly distributed along the length of the frame 5 and has a thickness of $t_{core} = 3 \cdot 10^{-4}$ m. The frame 5 has holes 7 designed for free circulation of the coolant. The coolant 8 (distilled water) is poured to the level of the upper end of the frame 5, and its volume is 4.5 ml. Above the core, close to frame 5, a porous wick 9 made of mesh (100 mesh) is installed, made of non-magnetic stainless steel AISI 304 (wire diameter $d_w = 114 \cdot 10^{-6}$ m, hole size $d_h = 149 \cdot 10^{-6}$ m, porosity $\phi_{wick} = 0{,}7$) with a length of 450 mm. The wick has four full turns, tightly adjacent to each other, with a total thickness of $t_{wick} \approx 1 \cdot 10^{-4}$ m. At the upper end of the tube 1, above the porous wick 9, the vacuum valve body 10 is soldered, the fastener 11 of which is installed on a caprolon gasket 12.

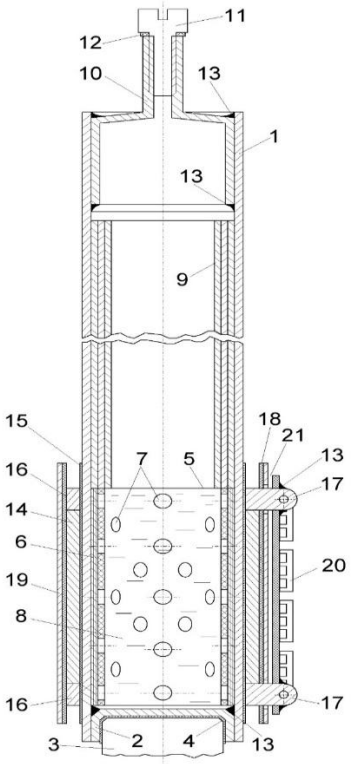

Fig. 1. Design of a heat pipe with induction heating.

Number 13 indicates the soldering points in the heat pipe casing.

To achieve a low temperature difference along the surface of the heat pipe, the working pressure of saturated steam inside it is 12.3 kPa at a temperature of 50°C.

A cylindrical inductance coil 14 is used for induction heating of the core 6 with high-frequency currents. Coil 14 is wound in the lower part of the heat pipe on an insulating layer 15 made of heat-conducting heat-resistant silicone compound SE 4486 from DOW with a thermal conductivity of 1.9 W/(m·K) [6] with a thickness of 0.1 mm and contains 100 turns of PEV-2-0.25 copper wire [7]. Current is supplied to coil 14 through current-carrying rings 16 using terminals 17. Externally, the coil is covered with a layer 18 of Sinteflex 515 composite electrical insulation material [8], which is wrapped in two layers of copper foil 19, each 0.1 mm thick, to shield the coil. Holes are made in the electrical insulating material 18 and screen 19 for the current-carrying terminals 17, which, in order to reduce the length of the communication lines, are soldered directly to the induction heating control board 20, which is powered by an external signal generator. The board 20 has conductive tracks only on the upper side, to which radio elements are directly soldered. The lower side of the board is completely covered with foil, which is connected to the 'ground' terminal to protect against interference. The air gap 21 allows the temperature of the board to be reduced by free air circulation. The open part of the heat pipe, which participates in heat exchange $l_0 = 0{,}45$ m.

During heat transfer in a heat pipe with a porous wick, certain temperature differences arise, which can be expressed in terms of the equivalent thermal resistances of the corresponding electrical links [9-11].

Fig. 2 shows the transverse temperature differences that arise along one side of the heat pipe 1 with a core 2 placed on a frame with holes 3 and a porous wick 4 placed horizontally, during the transfer of external heat flow Q_I through the steam channel 5 from the evaporation zone to the condensation zone.

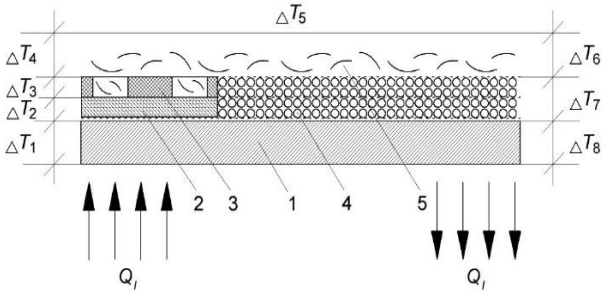

Fig. 2. Temperature differences along the length of a tube with a porous wick.

Fig. 3 shows the equivalent electrical circuit of thermal resistances that arise during the operation of the tube in Fig. 2. The direction of the heat flow Q_I is chosen as the direction of current flow.

Heat is removed from the surface of the heat pipe by convection and thermal radiation [9, 10]. Additional temperature differences appear in the evaporation and condensation zones due to heat transfer by thermal conductivity through the walls of the heat pipe. Thermal resistances also exist at the liquid-vapour interface and in the vapour core of the pipe [10-12].

The following symbols are used in Fig. 3: $R_{wall.e}$ and

$R_{wall.c}$ – thermal resistances of the heat pipe wall in the evaporation and condensation zones, K/W; R_{core} – thermal resistance of the core, K/W; R_{frame} – thermal resistance of the frame, K/W; $R_{p.t.e}$ and $R_{p.t.c}$ – thermal resistances of the phase transition from liquid to vapour in the evaporation and condensation zones, K/W; $R_{wick.c}$ – thermal resistance of the porous wick saturated with working fluid in the condensation zone, K/W; R_{evap} – thermal resistance of the vapour flow, K/W.

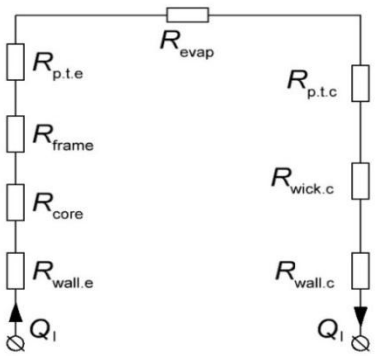

Fig. 3. Equivalent thermal resistances of a heat pipe under the action of a heat flux Q_l.

The total thermal resistance of the tube is found from the expression:

$$R_{total.} = R_{wall.e} + R_{core} + R_{frame} + R_{p.t.e} + R_{evap} + R_{p.t.c} + R_{wick.c} + R_{wall.c} \quad (1)$$

To calculate thermal resistance in a working heat pipe, we will use the following dependencies [9]:

$$R_{wall.e} = \frac{\ln\left(\frac{r_{in}+t_{wall}}{r_{in}}\right)}{2\cdot\pi\cdot\lambda_m\cdot l_{evap}}, \quad (2)$$

where l_{evap} is length of the evaporation zone, m; λ_m is thermal conductivity of the heat pipe wall material;

$$R_{core} = \frac{\ln\left(\frac{r_{in}}{r_{in}-t_{core}}\right)}{2\cdot\pi\cdot\lambda_{core}\cdot l_{evap}}, \quad (3)$$

where λ_{core} is thermal conductivity of the core material, W/(m·K).

To evaluate the effective thermal conductivity of the core, a model of successive layers was used, which is more realistic for a structure where the layers are arranged in sequence to the action of the heat flow. Typical porosity values for such cores range from 20% to 40%. Let us take the average porosity of the coolant to be, $\phi_l \approx 30\%$ then the volume fraction of steel is $\phi_{core} \approx 70$ %:

$$\frac{1}{\lambda_{core}} = \frac{\varphi_{core}}{\lambda_{AISI430}} + \frac{\varphi_l}{\lambda_l}, \quad (4)$$

where λ_l is thermal conductivity of the working fluid, W/(m·K); $\lambda_{AISI430}$ is thermal conductivity of the core material, W/(m·K);

$$R_{frame} = \frac{\ln\left(\frac{r_{in}-t_{core}}{r_{in}-t_{core}-t_{frame}}\right)}{2\cdot\pi\cdot\lambda_{frame}\cdot l_{evap}}, \quad (5)$$

where λ_{frame} is thermal conductivity of the frame material, W/(m·K);

$$R_{p.t.e} = \frac{1}{h_{evap}\cdot A_{evap}} = \frac{1}{h_{evap}\cdot 2\cdot\pi\cdot r_{in}\cdot l_{evap}}, \quad (6)$$

where h_{evap} is heat transfer coefficient during liquid-vapour phase transition, W/(m^2·K) [13];

$$R_{evap} = \frac{\mu_{steam}\cdot l_o}{\rho_{steam}\cdot A_{steam}\cdot r^2_{vap}\cdot L_{liquid}}, \quad (7)$$

where μ_{steam} is dynamic viscosity of steam, Pa·s; ρ_{steam} is density of steam, kg/m^3; A_{steam} is cross-sectional area of the steam channel, m^2; $A_{steam} = \pi \cdot r^2{}_{vap}$, r_{vap} is radius of the steam channel, m; $r_{vap} = r_{in} - t_{wick}$, m; L_{liquid} is latent heat of evaporation, J/kg;

$$R_{p.t.c} = \frac{1}{h_{cond}\cdot A_{cond}} = \frac{1}{h_{cond}\cdot 2\cdot\pi\cdot r_{in}\cdot l_{cond}\cdot\varphi_{wick}}, \quad (8)$$

where h_{cond} is heat transfer coefficient during vapour-liquid phase transition, W/(m^2·K) [13]; l_{cond} is length of the condensation zone, $l_{cond} = 0.45$ m;

$$R_{wick.c} = \frac{ln\left(\frac{r_{in}}{r_{vap}}\right)}{2\cdot\pi\cdot\lambda_{eff}\cdot l_{cond}}, \quad (9)$$

$$\lambda_{eff} = \lambda_l \cdot \frac{2\cdot\lambda_l+\lambda_{wick}-2\cdot\varphi_{wick}\cdot(\lambda_l-\lambda_{wick})}{2\cdot\lambda_l+\lambda_{wick}+\varphi_{wick}\cdot(\lambda_l-\lambda_{wick})}, \quad (10)$$

where λ_{wick} is thermal conductivity of porous wick, W/(m·K);

$$R_{wall.c} = \frac{ln\left(\frac{r_{in}+t_{wall}}{r_{in}}\right)}{2\cdot\pi\cdot\lambda_m\cdot l_{cond}} \quad (11)$$

The temperature difference between the evaporation and condensation zones, taking into account the cross-section of the heat pipe, is determined by the formula:

$$\Delta T = R_{total} \cdot Q \quad (12)$$

The data for calculating the thermal parameters of the tube are given in Table 1.

The calculation of model parameters using the above formulas is shown in Table 2.

Let us calculate the maximum heat flux that a heat pipe can transfer in bubble boiling mode at a given vapour temperature. We will use the calculation method given in [14].

Table 1.

Data values for calculating tube parameters

Parameter	Meaning	Unit of measurement
λ_m	390	W/(m·K)
λ_l	0.643	W/(m·K)
$\lambda_{AISI430}$	26.1	W/(m·K)
λ_{frame}	1.3	W/(m·K)
λ_{wick}	0.784	W/(m·K)
h_{evap}	4000	W/(m²·K)
r_{vap}	$7 \cdot 10^{-3}$	m
μ_{steam}	$9.65 \cdot 10^{-6}$	Pa·s
ρ_{steam}	0.094	kg/m³
A_{steam}	$1.54 \cdot 10^{-4}$	m²
L_{liquid}	2300000	J/kg
h_{cond}	6000	W/(m²·K)

Table 2.

Calculated tube parameters

Parameter	Meaning	Unit of measurement
λ_{core}	2.03	W/(m·K)
$R_{wall.e}$	0.0016	K/W
R_{core}	0.1	K/W
R_{frame}	0.162	K/W
$R_{p.t.e}$	0.147	K/W
R_{evap}	0.0091	K/W
$R_{p.t.c}$	0.0105	K/W
$R_{wick.c}$	0.06	K/W
λ_{eff}	2.03	W/(m·K)
$R_{wall.c}$	0.00106	K/W
R_{total}	0.491	K/W
ΔT	4.91	K

To ensure normal operation of the heat pipe in bubble boiling mode, the maximum capillary pressure must be greater than or equal to the sum of the pressure drops that occur in the heat transfer system. This allows the liquid to circulate freely inside the pipe, overcoming all resistance [15]. This condition is described by the following formula [14]:

$$(\Delta p_k)_{max} \geq \Delta p_g + \Delta p_{liquid} + \Delta p_{steam}, \quad (13)$$

where $(\Delta p_k)_{max}$ is maximum capillary pressure, Pa; Δp_g is gravitational component of total pressure drop, Pa; Δp_{liquid} is pressure drop in the fluid flow (heat carrier), Pa; Δp_{steam} is pressure drop in the steam flow, Pa.

When determining the minimum flow rate of the working fluid that will ensure the transfer of the required heat flow, the pressure drop in the steam flow can be neglected.

The components of expression (13) are calculated according to the following dependencies:

$$\Delta p_k = \frac{2 \cdot \sigma_{liquid}}{r_{pore}} \cdot cos\,\theta, \quad (14)$$

where σ_{liquid} is surface tension of the working fluid, N/m; $cos\,\theta$ is contact angle; r_{pore} is effective radius of the pore wall, m.

$$\Delta p_g = \rho_{liquid} \cdot g \cdot l_o \cdot sin\,\varphi, \quad (15)$$

where ρ_{liquid} is density of the working fluid, kg/m³; g is acceleration due to gravity, m/s²; φ is angle of inclination of the heat pipe, degrees;

$$\Delta p_{liquid} = \frac{\mu_{liquid} \cdot l_o \cdot Q_{max}}{K_{wick} \cdot A_{wick} \cdot \rho_{liquid} \cdot L_{liquid}}, \quad (16)$$

where μ_{liquid} is viscosity of the working fluid, N·s/m²; A_{wick} is cross-sectional area of the heat pipe wick, m².

The maximum permissible heat flow that a heat pipe can transfer in pre-crisis heat exchange mode is calculated using the following formula:

$$Q_{max} = m_{max} \cdot L_{liquid}, \quad (17)$$

where m_{max} is working fluid consumption in the nozzle at maximum steam temperature, kg.

The expression for calculating the working fluid flow rate in the wick at maximum steam temperature m_{max} is obtained by making the following assumptions:

– the properties of the working fluid along the tube are constant;

– the pressure drop in the steam flow is negligible;

– the structure of the wick is homogeneous.

Hence

$$m_{max} = \frac{\rho_{liquid}}{\mu_{liquid}} \cdot \frac{K_{wick} \cdot A_{wick}}{l_o} \left(\frac{\sigma_{liquid}}{r_{pore}} \cdot cos\,\theta - \rho_{liquid} \cdot g \cdot l_o \cdot sin\,\varphi \right) \quad (18)$$

To calculate this, we will use the parameters given for experimental heat pipes in [1] ($Q = 10$W, $T = T_{max} = 50$°C), the characteristics of distilled water at a temperature of 50 °C [16], given in Table 3, and the conditions of ideal wetting, when $\theta = 0°$. The permeability for the selected type of wick, according to the Kozeni-Karmann equation, is $K_{wick} = 1.61 \cdot 10^{-11}$ m². Then $A_{wick} = 3.14 \cdot (r_{in}{}^2 - r_{vap}{}^2) = 3.14 \cdot ((8 \cdot 10^{-3})^2 - (7 \cdot 10^{-3})^2) \approx 4.7 \cdot 10^{-5}$ m².

The pore radius is found from the empirical expression [17]:

$$r_{pore} \approx \frac{d_w \cdot S_w}{8}, \quad (19)$$

where S_w is specific window ratio, which for a 100 mesh grid and 0.114 mm wire is ≈ 0.5;

$$r_{pore} \approx \frac{0{,}000114 \cdot 0.5}{8} \approx 7.13 \cdot 10^{-6} m.$$

The calculation m_{max} and Q_{max} for φ from 0° to 90° with a resolution of 10° is given in Table 4.

The calculation of the tube parameters to satisfy condition (13) is given in Table 5.

Table 3.

Properties of the heat tr/ansfer fluid at 50 °C [16]

L_{liquid}, MJ/kg	ρ_{liquid}, kg/m^3	μ_{liquid}, N·sm^2	σ_{liquid}, N/m	λ_l, W/(m·K)
2.38	988	0.000547	0.0679	0.643

Table 4.

Calculation results m_{max} and Q_{max} at different tube inclination angles

φ, degrees	0	10	20	30	40	50	60	70	80	90
m_{max}, kg	2.9× ×10^{-5}	2.85× ×10^{-5}	2.72× ×10^{-5}	2.5× ×10^{-5}	2.22× ×10^{-5}	1.86× ×10^{-5}	1.45× ×10^{-5}	9.89× ×10^{-6}	5.03× ×10^{-6}	0
Q_{max}, W	68.8	67.8	64.7	59.6	52.7	44.3	34.4	23.5	12	0

Table 5.

Verification of condition (13) at different angles of inclination of the heat pipe

φ, degrees	Δp_g, Pa	Δp_{liquid}, Pa	Δp_k, Pa	Fulfilment of condition (13)
0°	0	9517.7	19038.2	Yes
10°	758.9	9379.3	19038.2	Yes
20°	1491.64	8950.5	19038.2	Yes
30°	2180.8	8245	19038.2	Yes
40°	2804.5	7290.4	19038.2	Yes
50°	3340.9	6128.4	19038.2	Yes
60°	3777.1	4758.8	19038.2	Yes
70°	4099.8	3250.9	19038.2	Yes
80°	4296.1	1660.1	19038.2	Yes
90°	4361.5	0	19038.2	-

The calculations showed that the designed tube is capable of effectively transferring a heat flux of up to 10 W. The calculated maximum power (Q_{max}) significantly exceeds the specified value (68.8 W versus 10 W in a practically horizontal position), which indicates a high safety margin and stability of its operation.

Verification of the capillary limit (condition (13)) confirmed that the tube can operate normally at angles of inclination from 0° to 70°. However, as calculations show, at angles of inclination close to the vertical position (over 80°), the capillary pressure becomes insufficient to ensure the circulation of the working fluid. This leads to a significant reduction in fluid flow, which in turn causes a heat exchange crisis and cessation of heat transfer, as demonstrated by Q_{max} approaching zero.

Thus, the designed heat pipe is reliable and effective within the specified power range (up to 10 W) at angles of inclination up to 70°.

To ensure reliable operation of the heat pipe at angles of inclination exceeding 80°, the following must be done:

– use a wick structure with a smaller pore radius and higher capillary pressure;

– increase the thickness or number of wick mesh layers to reduce hydraulic resistance;

– use a working fluid with a lower surface tension coefficient and greater surface wetting ability;

– organise additional cooling in the condensation zone.

Let us calculate the parameters of the induction heating system of the heat pipe. From the design shown in Fig. 1, the inductance of a single-layer cylindrical coil can be determined using a simplified formula [18,19]:

$$L_{coil} = \mu \cdot \frac{N^2 \cdot A_{coil}}{l_{coil}}, \quad (20)$$

where L_{coil} is coil inductance (H); μ is absolute magnetic permeability of the coil core (H/m); N is number of coil turns (pcs.); A_{coil} is coil cross-sectional area (m^2); l_{coil} is coil length (m).

Absolute magnetic permeability is calculated as $\mu = \mu_r \cdot \mu_0$, where μ_r is the relative magnetic permeability of the core material; μ_0 is the magnetic permeability of a vacuum, equal to $4\pi \cdot 10^{-7}$ H/m.

The core material AISI 430 is ferritic stainless steel, which has ferromagnetic properties [20]. Its relative magnetic permeability can vary significantly depending on the specific condition of the material (annealed, cold-rolled) and the intensity of the magnetic field. However, for average values, values in the range from 100 to 1000 are often indicated [21,22]. Based on practical studies conducted for AISI 430 steel strips, we will take the average value of relative magnetic permeability $\mu_r = 300$. Hence $\mu = 300 \cdot 4 \cdot 3.14 \cdot 10^{-7} = 3.77 \cdot 10^{-4}$ H/m [23,24].

The number of coil turns is *N*=100. The coil is wound on a heat pipe with a diameter of $D_{o.p.} = 18$ mm, on top of a layer of insulating heat-conducting compound with a thickness of 0.1 mm. Therefore, the diameter of the coil is $D_{coil} = D_{o.p.} + 0.1 \cdot 2 = 18 + 0.2 = 18.2$ mm, or 0.0182 m. The length of the coil wire is:

$$l_w = \pi \cdot D_{coil} \cdot N = 3.14 \cdot 0.0182 \cdot 100 = 5.72 \text{ m}. \quad (21)$$

Given that the resistance of the PEV-2-0.25 wire is $R_w = 0.357$ Ohm·m, we can find the total resistance of the inductance coil:

$$R_{coil} = l_w \cdot R_w = 5.72 \cdot 0.357 = 2.04 \approx 2 \text{ Om} \quad (22)$$

The coil has a length of $l_{coil} = 30$ mm and is positioned symmetrically to the centre of the core 6 for better flux coupling.

The cross-sectional area of the coil is found from the

expression [24,25]:

$$A_{coil} = \pi \cdot \left(\frac{D_{coil}{}^2}{4}\right) = 3.14 \cdot \left(\frac{0.0182^2}{4}\right) = 2.6 \cdot 10^{-4} m^2 \quad (23)$$

Now let's substitute the values of the corresponding quantities into the formula (20):

$$L_{coil} = 3.77 \cdot 10^{-4} \cdot \frac{100^2 \cdot 2.6 \cdot 10^{-4}}{0.03} \approx 0.0327 \text{ H} \approx 32.7 \text{ mH}.$$

For efficient and rapid heating of thin-walled magnetic stainless steel cores using an induction coil, it is important to select the optimal frequency [26]. This frequency is determined by the depth of current penetration into the material δ - the thickness of the layer in which the induced currents are concentrated and effectively converted into heat. It is calculated using the formula [27,28]:

$$\delta = \sqrt{\frac{2\rho}{\omega\mu}} = \sqrt{\frac{2\rho}{2\pi f\mu}} = \sqrt{\frac{\rho}{\pi f\mu}} \quad (24)$$

where δ is current penetration depth (m); ρ is specific resistance of the material (Ohm·m); f is frequency (Hz).

For the most effective induction heating, the depth of current penetration must be less than the thickness of the core wall [29]. This will ensure maximum current concentration in the material and, as a result, the fastest heating. Therefore, considering the core thickness of 0.3 mm, we will choose $\delta \approx 0{,}15$ mm.

From expression (24) we obtain the formula for the optimal excitation frequency of the coil:

$$f = \frac{\rho}{\pi \cdot \mu \cdot \delta^2} \quad (25)$$

For AISI 430 steel, let's take an average value of $\rho \approx 7.5 \cdot 10^{-7}$ Ohm·m, then:

$$f = \frac{7.5 \cdot 10^{-7}}{3.14 \cdot 3.77 \cdot 10^{-4} \cdot 0.00015^2} = 28158 \approx 28.16\, kHz.$$

The total resistance of the coil at the optimum excitation frequency is [30,31]:

$$Z_{coil} = \sqrt{R_{coil}^2 + X_{L_{coil}}^2} = \sqrt{R_{coil}^2 + (2\pi f L_{coil})^2} = \sqrt{2.04^2 + (2 \cdot 3.14 \cdot 28158 \cdot 32.7 \cdot 10^{-3})^2} = 76.1\, Ohm \quad (26)$$

and is practically equal to its reactive resistance, because $X_{L_{coil}} \gg R_{L_{coil}}$.

This means that the active power used to heat the coil wire will be minimal compared to the reactive power. High inductive resistance is normal for inductive loads and is the reason for using a resonant circuit. Therefore, to compensate for reactive power, we connect a capacitor in parallel to the coil, creating a parallel resonant circuit. The current consumed from the power source at resonance will be minimal, but the currents circulating between the inductance and capacitance inside the circuit will be maximal due to the resonance of the currents [32]. The high voltage of the resonant circuit will create a powerful magnetic field that will increase the efficiency of the induction heating of the core.

The formula for calculating the resonance frequency is as follows:

$$f_{\text{p}} = \frac{1}{2\pi\sqrt{L_{coil} \cdot C}} \quad (27)$$

Given the condition that $f = f_p$, the capacitance of the capacitor is determined by the expression:

$$\text{C} = \frac{1}{(2\pi f)^2 \cdot L_{coil}} = \frac{1}{(2 \cdot 3.14 \cdot 28158)^2 \cdot 32.7 \cdot 10^{-3}} \approx 9.78 \cdot 10^{-10} = 978\, pF. \quad (28)$$

At the resonant frequency, the reactive resistances of inductance and capacitance are compensated, and the total resistance of the circuit is equal to its active resistance. Thus $Z_0 = R_{coil} = 2$ Ohm.

To determine the required circuit current, we need to start from the power required to heat the core, which, according to the data given in [1], is 10 W.

To calculate the supply voltage of the resonant circuit, we will use the expression for determining power:

$$P_0 = I^2 \cdot R_{coil}, \quad (29)$$

Where $I = \sqrt{\frac{P_0}{R_{coil}}} = \sqrt{\frac{10}{2}} \approx 2.23\, A$.

The significant current flowing through the conductor of the inductance coil will not cause its insulation to break down, as excess heat is effectively dissipated by the surface of the heat pipe.

The supply voltage of the resonant circuit is determined by Ohm's law:

$$U_p = \frac{P_0}{I} = \frac{10}{2.23} = 4.48 \approx 4.5 \text{ V}.$$

However, considering the voltage drop across the open circuit control transistor (approximately 0.5 V), we can assume $U_p = 5$ V.

Based on the results of calculations in Multisim 14.3, a two-transistor control circuit for an induction heater of a heat pipe was modelled, consisting of a parallel resonant circuit calculated above. Due to the low supply voltage of the circuit, field-effect transistors with 5 V logic level control were selected. For simplicity of implementation, the circuit was excited by rectangular pulses from the generator. The oscillograms obtained at the resonance frequency (Fig. 4) showed the correct operation of the

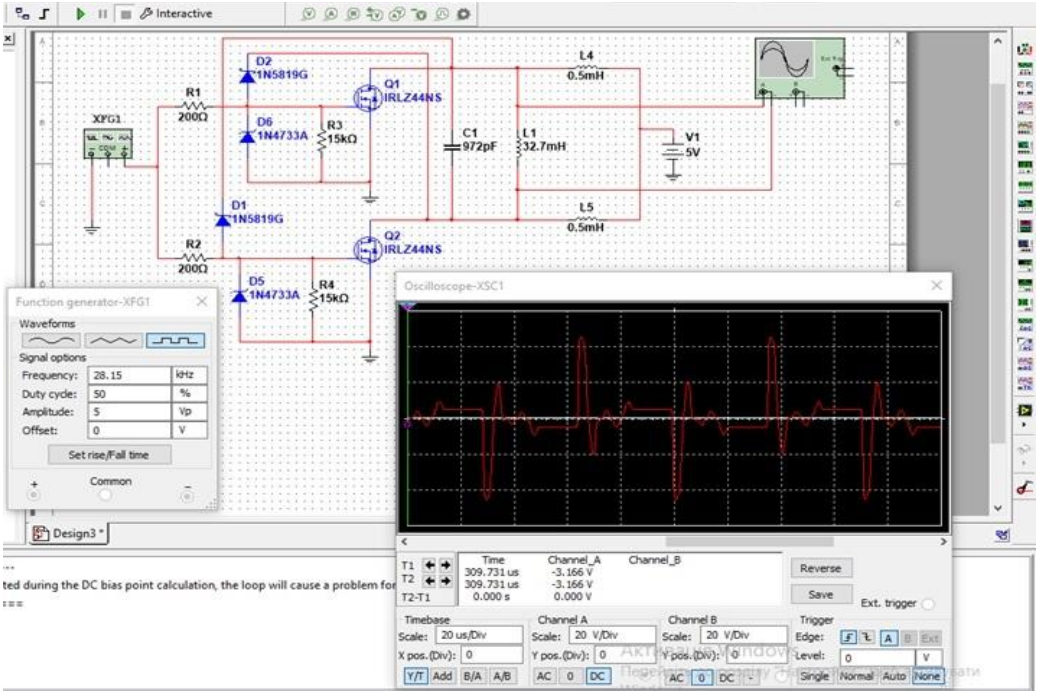

Fig. 4. Modelling of the induction heating system in Multisim 14.3.

induction heating system and the possibility of practical implementation of the control circuit powered by a power bank.

Conclusions

The paper presents a theoretical and computational study of a low-temperature wick heat pipe with induction heating of the core located inside it, which is designed for rapid heat transfer to the working fluid. A mathematical model of the heat balance was constructed, taking into account induction heating, the heat capacity of the elements, and heat transfer during free convection. The calculated maximum power of the heat pipe significantly exceeds the specified value (68.8 W in a vertical position versus 10 W in a horizontal position), which indicates a significant margin of safety and high stability of operation.

The dependence of the heating time and maximum thermal power on the angle of inclination of the heat pipe has been determined. It has been shown that in a vertical position, heat transfer efficiency is maximised due to the optimal operation of the wick structure and natural circulation of the coolant. Normal pipe operation occurs at angles of inclination up to 70°. When the tube is tilted up to 80°, operability is maintained, but efficiency gradually decreases due to an increase in gravitational resistance to the movement of the working fluid.

For reliable operation of the heat pipe at angles of inclination greater than 80°, it is necessary to use a wick with a smaller pore radius and higher capillary pressure, increase the number of mesh layers or their thickness, use a working fluid with a lower surface tension coefficient and greater ability to wet the surface instead of distilled water, and organise additional cooling in the condensation zone.

The elements of the induction heating system and the parameters of the oscillating circuit have been calculated. The system has been simulated in Multisim 14.

The results of calculations and modelling showed that the design of the heat pipe and the induction heating system of the coolant are effective and reliable. The proposed design has a significant safety margin and operates stably over a wide range of angles of inclination. The electrical part of the system, based on a parallel resonant circuit, ensures high heating efficiency with minimal power losses. These theoretical conclusions provide a reliable basis for moving on to the second part of the work, devoted to the creation of a test rig and experimental confirmation of the results obtained.

Vashchyshak I.R. – Candidate of Technical Sciences, Associate Professor of the Department of information and measurement technologies and energy management;
Vashchyshak S.P. – Candidate of Technical Sciences, Associate Professor, Head of the Department of Information Technologies;
Mazur T.M. – Doctor of Philosophy, Associate Professor of the Department of Physical and Mathematical Sciences;
Mazur M.P. – Associate Professor, Ph.D (Physics and Mathematics), Dean of the Faculty of Automation and Energy.

[1] I. Vashchyshak, S. Vashchyshak, T. Mazur, & M. Mazur, *Study of the influence of the environment on the efficiency of induction heating of low-temperature heat pipe,* Physics and Chemistry of Solid State, 5(4), 787–794 (2024); https://doi.org/10.15330/pcss.25.4.787-794.

[2] Mrs. J. Emeema. Heat Pipes – *A Review on Performance Parameters*. International Journal of Creative Research Thoughts, 6(2), 746 (2018); https://ijcrt.org/papers/IJCRT1892456.pdf.
[3] V. Agarwal, S. Jain, K. Vya, G. Jain, *A Review Paper on Role of Heat Pipes in Cooling*, International Journal of Emerging Trends in Electrical and Electronics, 11(2), 154 (2015); https://www.academia.edu/29562085/A_Review_Paper_on_Role_of_Heat_Pipes_in_Cooling_CTAE_1_2_GITS_3_4?uc-g-sw=85697005.
[4] I.R. Vashchyshak, *Multi-fuel boiler with heat pipes*. Scientific Bulletin of UNFU, 28(1), 74 (2018). https://doi.org/10.15421/40280115.
[5] AZOM. S-Glass Properties, Electronic resource; https://www.azom.com/properties.aspx?ArticleID=769.
[6] Dow Corning. SE 4486 CV 330ml, Electronic resource; https://octopart.com/datasheet/se+4486+cv+330ml-dow+corning-8663911.
[7] Enameled wire PEV-2-0.25, Electronic resource; Режим доступу: https://archive.org/details/B-001-014-096/page/14/mode/2up.
[8] Syntoflex 515, Electronic resource; https://tantal-td.prom.ua/ua/p1130399510-sintofleks-515-025.html.
[9] G.P. Peterson, An Introduction to Heat Pipes: Modeling, Testing, and Applications. New York: Wiley, 352 (1994); https://scispace.com/papers/an-introduction-to-heat-pipes-modeling-testing-and-2y3lhct4sj?citations_page=3.
[10] A.V. Hilchuk, A.A. K halatov, T.V. Donyk, Teoriia teploprovidnosti. Kyiv: KPI im. Ihoria Sikorskoho, 248 (2022); https://ela.kpi.ua/server/api/core/bitstreams/f2c859d5-be0b-486f-80c1-7e3fc320b662/content.
[11] B. Dzundza, O. Kostyuk, & T. Mazur, *Software and Hardware Complex for Study of Photoelectric Properties of Semiconductor Structures.* 2019 IEEE 39th International Conference on Electronics and Nanotechnology (ELNANO), Kyiv, 16-18 April, (2019); https://doi.org/10.1109/ELNANO.2019.8783544.
[12] B.S. Dzundza, V.V. Prokopiv, T.M. Mazur, L.D. Yurchyshyn, *Automation of measurements of photoelectric parameters of high-impedance semiconductor films.* Physics and chemistry of solid state, 19(4), 363-367 (2018); https://doi.org/10.15330/pcss.19.4.363-367.
[13] A. Faghri, Heat Pipe Science and Technology. Washington: Taylor & Francis, 832 (1995); https://www.scirp.org/reference/referencespapers?referenceid=1987184.
[14] D.A. Reay, P.A. Kew, R.J. McGlen, Heat Pipes: Theory, Design and Applications. 6th ed. Oxford: Butterworth-Heinemann, 432 (2014); https://pdfcentro.com/library/heat-pipes-theory-design-and-applications-4971452.
[15] K. Blauciak, P. Szymanski, & D. Mikielewicz, *The Influence of Loop Heat Pipe Evaporator Porous Structure Parameters and Charge on Its Effectiveness for Ethanol and Water as Working Fluids*. Materials, 14(22), 7029 (2021); https://doi.org/10.3390/ma14227029.
[16] NIST Chemistry WebBook/NIST Standard Reference Database Number 69; https://doi.org/10.18434/T4D303.
[17] Y.P. Pao, *Fluid Mechanics*. New York: John Wiley & Sons, 512 (1981); https://www.abebooks.com/Fluid-Mechanics-Pao-Richard-H.F-John/31424906055/bd.
[18] J.D. Kraus, Electromagnetics. New York: McGraw-Hill, 672 (1992); https://www.academia.edu/22648236/ELECTROMAGNETICS_SIMPLY_EXPLAINED.
[19] F.T. Ulaby, *Fundamentals of Applied Electromagnetics*. Boston: Pearson, 832 (2015); https://mrce.in/ebooks/Electromagnetics%20(Applied)%20Fundamentals%208th%20Ed.pdf.
[20] Y. Kusyi, V. Stupnytskyy, O. Kostiuk, O. Onysko, E. Dragašius, S. Baskutis, R. Chatys. *Control of the parameters of the surface layer of steel parts during their processing applying the material homogeneity criterion*. Eksploatacja i Niezawodnosc, 26 (3), 187794 (2024); https://doi.org/10.17531/ein/187794.
[21] ASM Handbook. Vol. 1: Properties and Selection: Irons, Steels and High-Performance Alloys. Materials Park, OH: ASM International, 1024 (1990); https://doi.org/10.31399/asm.hb.v01.9781627081610.
[22] B.D. Cullity, C.D. Graham, *Introduction to Magnetic Materials*. Hoboken, NJ: Wiley-IEEE Press, 608 (2011); https://www.wiley.com/en-us/Introduction+to+Magnetic+Materials%2C+2nd+Edition-p-9781118211496.
[23] D.J. Griffiths, *Introduction to Electrodynamics*. Boston: Pearson, 840 (2014); https://books.google.com/books/about/Introduction_to_Electrodynamics.html?id=J9ygBwAAQBAJ.
[24] E. Kreyszig, *Advanced Engineering Mathematics*. Hoboken, NJ: Wiley, 1 024 (2011); http://www.uop.edu.pk/ocontents/AdvancedEngineeringMathematics.pdf.
[25] F. Beer, E.R. Johnston, *Vector Mechanics for Engineers*. New York: McGraw-Hill, 920 (2006); https://www.mheducation.com/highered/product/Vector-Mechanics-for-Engineers-Statics-and-Dynamics-Beer.html.
[26] O. Onysko, V. Kopei, C. Barz, Y. Kusyi, S. Baskutis, M. Bembenek, P. Dašić, V. Panchuk. *Analytical Model of Tapered Thread Made by Turning from Different Machinability Workpieces*. Machines, 12(5), 313(2024); https://doi.org/10.3390/machines12050313.
[27] S. Ramo, J. R. Whinnery, T. Van Duzer, Fields and Waves in Communication Electronics. New York: Wiley, 864 (1994); https://www.wiley.com/en-us/Fields+and+Waves+in+Communication+Electronics%2C+3rd+Edition-p-9780471585510.
[28] R.F. Harrington, *Time-Harmonic Electromagnetic Fields. Hoboken*, NJ: Wiley-IEEE Press, 560 (2001); https://www.scirp.org/reference/referencespapers?referenceid=418936.

[29] Xuecheng Fu, Mingyang Ma, Shumiao Wang, Chunming Teng, Wenfeng Liang, *Heat generation and transfer simulation of a high temperature heat pipe under induction heating based on a coupled model*, Applied Thermal Engineering, 232, (2023); https://doi.org/10.1016/j.applthermaleng.2023.121025.

[30] A.E. Fitzgerald, C. Kingsley, S.D. Umans, *Electric Machinery*. New York: McGraw-Hill, 736 (2003); https://mrce.in/ebooks/Electric%20Machinery%20Fitzgerald%20&%20Kingsley%E2%80%99s%207th%20Ed.pdf.

[31] P.C. Sen, *Principles of Electric Machines and Power Electronics*. New York: Wiley, 512 (2014); https://mrce.in/ebooks/Electric%20Machines%20&%20Power%20Electronics%20Principles%203rd%20Ed.pdf.

[32] P. Szymanski, D. Mikielewicz, & S. Fooladpanjeh, *Current Trends in Wick Structure Construction in Loop Heat Pipes Applications: A Review.* Materials, 15(16), 5765 (2022); https://doi.org/10.3390/ma15165765.

І.Р. Ващишак[1], С.П. Ващишак[2], Т.М. Мазур[1], М.П. Мазур[1]

Дослідження ефективності теплопередачі гнітової теплової трубки з індукційним нагріванням осердя з магнітної нержавіючої сталі

[1]Івано Франківський національний технічний університет нафти і газу, м. Івано-Франківськ, Україна, tetiana.mazur@nung.edu.ua

[2]Університет Короля Данила, м. Івано-Франківськ, Україна

Представлено результати математичного моделювання теплової трубки з індукційним нагрівом осердя, призначеної для ефективної передачі низькотемпературного теплового потоку робочій рідині в умовах обмежених габаритів. Розглянуто конструкцію, що включає тонкостінний корпус з міді, пористу гнітову структуру із сітки з немагнітної нержавіючої сталі та осердя з магнітної нержавіючої сталі, яке нагрівається за допомогою циліндричної індукційної котушки, розміщеної на корпусі над осердям. На основі фізичних моделей теплообміну розроблено математичний опис процесів, що враховує індукційне виділення тепла, теплоємність компонентів трубки та теплові втрати при вільній конвекції. Встановлено залежність динаміки нагріву та теплової ефективності від кута нахилу теплової трубки відносно вертикалі. Результати розрахунків показали, що при вертикальному розташуванні досягається максимальна ефективність, а зі збільшенням кута нахилу понад 60° спостерігається зростання гравітаційного опору руху рідини, що призводить до поступового зменшення теплопередачі. Показано, що при нахилах до 80° працездатність конструкції зберігається, однак для забезпечення стабільної роботи при ще більших кутах необхідні додаткові заходи: зменшення радіуса пор гнітової структури для підвищення капілярного тиску, збільшення товщини або кількості шарів сітки, а також підбір робочих рідин із більш сприятливими змочувальними властивостями. Подальші роботи спрямовані на експериментальну перевірку отриманих моделей та оптимізацію конструктивних параметрів для розширення діапазону робочих кутів нахилу.

Ключові слова: теплова трубка, осердя, термічний опір, тепловий потік, теплопровідність, резонансний контур, частота.